AIAA 2003–0776

LARGE EDDY SIMULATION APPLIED TO A HIGH-REYNOLDS FLOW AROUND AN AIRFOIL CLOSE TO STALL

S. Dahlström and L. Davidson
Department of Thermo and Fluid Dynamics
Chalmers University of Technology
SE-412 96 Göteborg, Sweden

41st AIAA Aerospace Sciences Meeting and Exhibit
6–9 January 2003 / Reno, NV

LARGE EDDY SIMULATION APPLIED TO A HIGH-REYNOLDS FLOW AROUND AN AIRFOIL CLOSE TO STALL

S. Dahlström and L. Davidson
Department of Thermo and Fluid Dynamics
Chalmers University of Technology
SE-412 96 Göteborg, Sweden

The subsonic flow ($Ma_\infty = 0.15$) around the Aerospatiale A-profile at an incidence of $13.3°$ and at a chord Reynolds number of $2 \cdot 10^6$ is studied using Large Eddy Simulation (LES). A wall-resolved LES of this flow is feasible, however it is of little interest if we want LES to be applicable on flows around three-dimensional bodies, such as a whole wing. In this paper steps towards a coarse LES method is taken. It includes handling the numerical problems at high Reynolds numbers (using a wiggle detector), finding ways of reducing the computational time (using parallelization and a 2D/3D approach) and investigations and discussions on the advantages of using a well-resolved LES outside the near-wall region, in the major part of the boundary layer. Unphysical oscillations are effectively dampened by the wiggle-detector scheme and the scheme is mostly central in the turbulent boundary layer. The LES resolution is good in the major part of the boundary layer (except in the near-wall region) and the transition mechanism is captured, which gives us hope that the overall flow is reasonable and useful information could be obtained on e.g. time variation of lift and drag. However, compared to the experiments, the laminar separation bubble is too large, leading to a delayed transition and an underpredicted lift force. The boundary layer thickness is linked to the size and the extent of the laminar bubble and the treatment of the laminar and transitional regions needs further investigations.

Introduction

The work presented in this paper is a continuation of the work carried out within the Brite-Euram project LESFOIL.[1–3] The airfoil case studied in the project is the flow around the Aerospatiale A-airfoil at an angle of attack, α, of $13.3°$. The chord Reynolds number is $2 \cdot 10^6$ and the flow is subsonic with a freestream Mach number of 0.15. In Fig. 1 experimental results are shown. The dashed line marks the $13.3°$-case, where the flow is near maximum lift and the airfoil is close to stall. The experiments have been performed by ONERA in wind tunnels F1 and F2.[4] It was seen that the following flow develops: at the leading edge there is a very thin laminar boundary layer. On the pressure side, this boundary layer is tripped at 30 % of the chord and there is a transition to a thin turbulent boundary layer. On the suction side, the favorable pressure gradient accelerates the flow around the leading edge, a separation bubble is formed in which transition takes place and the flow reattaches at approximately 12 % of the chord. The boundary layer grows under the influence of an adverse pressure gradient and, at about 82.5 % of the chord, the flow separates. The separation is weaker in the experiment in the F1 tunnel, where the separation occurs at approximately 95 % of the chord. That the flow is closer to stall in the F2 wind-tunnel measurements is also seen in Fig. 1. A too large blockage in the experimental setup in the F2 wind tunnel is probably the main reason for the difference between the two experiments.[4]

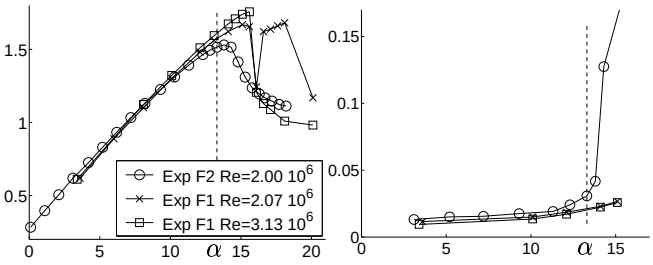

Fig. 1 Lift and drag coefficients versus the angle of attack.

This flow has been the subject of extensive studies. Different CFD codes (steady and unsteady RANS, compressible and incompressible methods) were validated in the EUROVAL project[5] and in the ECARP project[6] on this particular single-element airfoil. It was found that few RANS models are

capable of handling this flow problem, mainly because of the lack of curvature effects in the eddy-viscosity models. The second-moment closures (which do take into account curvature effects) produced the best results.[7–9]

Large Eddy Simulation (LES) of flows around airfoils have been conducted prior to the LESFOIL project, e.g. in a study on the NACA 4412 profile,[10] the present A-profile[11] and in extensive studies including compressible flow.[12] If we could have unlimited access to computer power, the ideal method would of course be Direct Numerical Simulation (DNS), since there is no modeling of unknown terms. Maybe LES could be classified as the "second best method" since it in the limit of finer and finer resolution becomes DNS. The questions are: what resolution is required and is LES a feasible method of computing flows around simple, 2D airfoils? The aim of the LESFOIL project was to investigate these questions. It has been demonstrated by ONERA that LES is feasible for incipient separation flows around 2D profiles.[13]

So, if this *very* 2D flow is feasible (in ONERA's work they used an extent of 1.5 % of the chord and a mesh consisting of 7.2 million nodes), what about the feasibility of LES for more three-dimensional flows around the profile (or e.g. around 3D wing sections)? With the present computer resources it is not feasible and therefore a lot of effort in the LESFOIL project was put into handling coarse meshes, using wall functions,[14,15] different ways of treating the transition[16] and DES.[17] Conclusions from previous work[15] lead us to investigate the coarse LES approach presented in this paper. Regarding the transition, conclusions were that it is difficult to prescribe the transition and that it rather should be a natural transition following a resolved laminar separation bubble. It was also suggested that the resolution should be approximately 200 wall units in the streamwise and spanwise direction in order to capture large-scale structures *outside* the near-wall region.[18] Today, when near-wall modeling for LES is not well understood, the requirements for coarse LES is investigated in the present approach. We cannot simply rely on a near-wall model as a replacement for a wall-resolved LES. The fundamental questions are: what are the advantages of having a LES model in the off-near-wall region, where the resolution is good and what are the advantages of using coarse LES in the transition region?

This is a challenging case owing to the high Reynolds number and because of the different flow regimes around the airfoil. Because of the strong coupling between the trailing edge separation and the pressure peak at the leading edge, all regions around the airfoil are probably equally important. This is often referred to as a close-to-the-trailing-edge problem although it could be the other way around. It is probably possible to get good velocity profiles close to the trailing edge, by using wrong laminar treatments, such as too high freestream turbulence, too dissipative schemes or other doubtful modifications. Of course, something needs to be done in the laminar region, e.g. we would rather have a dissipative scheme than wiggles that contaminate all of the domain. However, it is probably crucial that the treatment in the laminar region is correct and thus the numeric is important. One step towards a good scheme is the use of wiggle detectors. Wiggle detectors were used in the LESFOIL project[13,19] and a smooth version is now used in this work.

Numerical Method

The code used is an incompressible finite volume Navier-Stokes solver called CALC-BFC.[20] The solver is based on structured grids and the use of curvi-linear boundary fitted coordinates. The grid arrangement is collocated and the Rhie and Chow interpolation method is used.[21] The code is parallelized for 3D flows[22] using block decomposition and the message passing systems PVM and MPI. The PISO algorithm[23] is used for the pressure-velocity coupling, with two additional corrector steps beside the first SIMPLE step. The filtered momentum equations are discretized in time using the Crank-Nicolson scheme and in space using 2nd order difference schemes (a mix between the central difference scheme (CDS) and the van Leer scheme).

LES with a one-equation SGS model

In LES, the large eddies are solved and the small scales are modeled. Filtering of the incompressible continuity and momentum equations results in

$$\frac{\partial \overline{u}_i}{\partial x_i} = 0 \quad (1)$$

$$\frac{\partial \overline{u}_i}{\partial t} + \frac{\partial}{\partial x_j}(\overline{u}_i \overline{u}_j) = -\frac{1}{\rho}\frac{\partial \overline{p}}{\partial x_i} + \frac{\partial}{\partial x_j}\left[\nu \frac{\partial \overline{u}_i}{\partial x_j} - \tau_{ij}\right] \quad (2)$$

$$\tau_{ij} = \overline{u_i u_j} - \overline{u}_i \overline{u}_j \quad (3)$$

Here, τ_{ij} are the subgrid scale (SGS) stresses. They are the contribution of the small scales, the unresolved stresses, and are unknown and must be modeled.

The SGS model used in the computations is the one-equation SGS model by Yoshizawa.[24] This is a one-equation model for the kinetic energy of the unresolved stresses, k_{sgs}. It reads:

$$\frac{\partial k_{sgs}}{\partial t} + \frac{\partial}{\partial x_j}(\bar{u}_j k_{sgs}) = \tag{4}$$
$$\frac{\partial}{\partial x_j}\left[(\nu + \nu_{sgs})\frac{\partial k_{sgs}}{\partial x_j}\right] + P_{k_{sgs}} - C_\varepsilon \frac{k_{sgs}^{3/2}}{\Delta}$$

$$P_{k_{sgs}} = 2\nu_{sgs}\bar{S}_{ij}\bar{S}_{ij},\ \nu_{sgs} = C_k \Delta k_{sgs}^{1/2} \tag{5}$$

Here, $\overline{S}_{ij} = \frac{1}{2}\left(\frac{\partial \overline{u}_i}{dx_j} + \frac{\partial \overline{u}_j}{dx_i}\right)$ is the filtered strain rate. The filter width, Δ, is computed using the definition $\Delta^3 = \Delta x \Delta y \Delta z = \delta V$, i.e. Δ is taken as the cubic root of the volume of a finite volume cell. The constants are $C_k = 0.07$ and $C_\varepsilon = 1.05$.[25]

The unresolved stresses are modeled using the eddy-viscosity hypothesis:

$$\tau_{ij} - \frac{1}{3}\delta_{ij}\tau_{kk} = -2\nu_{sgs}\overline{S}_{ij} \tag{6}$$

This approach of modeling is known to produce erroneous results in the stagnation point region, known as the *stagnation point anomaly*. This can be improved, following Durbin, by using the *realizability constraint*, $0 \le \tau_{ll} \le 2k_{sgs}$ (no summation on l), upon the eddy viscosity via a bound on the time scale.[26] Here, the turbulent time scale, T, is taken as $k_{sgs}/\varepsilon_{sgs}$, where $\varepsilon_{sgs} = C_\varepsilon k_{sgs}^{3/2}/\Delta$. The SGS eddy viscosity in Eq. 5 can now be expressed as:

$$\nu_{sgs} = C_k C_\varepsilon k_{sgs} T \tag{7}$$

and the bound on T becomes:

$$T = \frac{1}{C_\varepsilon}\min\left(\frac{\Delta}{\sqrt{k_{sgs}}}, \frac{1}{C_k\sqrt{6\bar{S}_{ij}\bar{S}_{ij}}}\right) \tag{8}$$

Spatial scheme

The central difference scheme (CDS) is often used in LES because of its non-dissipative and energy-conserving properties. When the momentum equations are discretized in space using this scheme it can produce odd-even oscillations (grid-to-grid oscillations or wiggles) if the resolution is poor. In the present computations, to be able to remove unphysical oscillations, a bounded second-order upwind discretization scheme (the van Leer scheme) is mixed with the CDS. The schemes are blended and the convective flux can be expressed as:

$$\dot{m}u_{UDS}^m + \dot{m}\left[\alpha u_{CDS}^{m-1} - \alpha u_{UDS}^{m-1} + (1-\alpha)u_{UDScorr}^{m-1}\right], \tag{9}$$

for a face in the i-direction. Here, CDS stands for the central difference scheme, UDS for the 1st-order upwind scheme and $UDScorr$ for the 2nd-order correction to the lower order upwind scheme ($m-1$ is the previous iteration). Here α is a blending factor ($0 \le \alpha \le 1$) and, at the extremes, we have:

$\alpha = 0$: the van Leer scheme
$\alpha = 1$: the central difference scheme with deferred correction[27]

A wiggle detector has been implemented. It checks if a wiggle is present in the i-, j- or k-direction for any of the three velocities. If this is the case the scheme changes 1 % towards the van Leer scheme, i.e. $\alpha^{n+1} = \max(\alpha^n - 0.01, 0)$, where n denotes time step number. Otherwise the scheme is more centered and $\alpha^{n+1} = \min(\alpha^n + 0.01, 1)$.

It is not obvious what is an unphysical wiggle and what is turbulence. This is one reason for changing the scheme smoothly. Apart from this the wiggle definition is arbitrary and is chosen in order to minimize the numerical dissipation, without destabilizing the numerical procedure. In the present computations a wiggle is present in the l-direction ($l = i, j, k$), if the coefficient of direction changes twice from node to node in this direction (see Fig.2). That is, if (for any velocity Φ)

$$\begin{gathered}(\Phi_{l+1} - \Phi_l)(\Phi_l - \Phi_{l-1}) < 0 \\ \text{and} \\ (\Phi_{l+2} - \Phi_{l+1})(\Phi_{l+1} - \Phi_l) < 0\end{gathered} \tag{10}$$

is true, then a wiggle is present and α in the convective flux in Eq. 9 through face $l+1/2$ is modified ($\alpha^{n+1} = \max(\alpha^n - 0.01, 0)$).

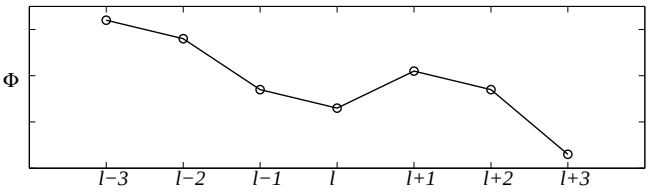

Fig. 2 The definition of a wiggle in the present computations. In this example there is an unphysical wiggle on face $l+1/2$, but not on face $l-1/2$.

Computational Setup

The Mesh

The computations have been conducted on a C-mesh consisting of 1393×127 nodes in the streamwise and wall-normal direction respectively (see Fig. 3). This mesh has been specially designed to give $y_1^+ < 1$. Special attention has also been given to keep half of the nodes in the wall-normal direction outside turbulent regions. Here the spanwise amount of nodes is 3, i.e. 2D simulation is performed in this region. In the 3D region, 33 nodes are used. This 2D/3D approach, which was used by ONERA,[13] enables us to save 45% of the nodes.

Table 1 shows some data on the mesh. The height of the cell at the leading edge is very small in order to resolve the laminar boundary layer.[18] The

# of grid nodes in the $i \times j \times k$-direction:	$1393 \times 64 \times 33 + 1393 \times 64 \times 3$
# of nodes along the wake in the i-direction:	110
# of nodes on the pressure side in the i-direction:	426
# of nodes on the suction side in the i-direction:	748
Length $\times$ height of the cell at the leading edge:	$1.0 \cdot 10^{-3}c \times 5.1 \cdot 10^{-6}c$
Length $\times$ height of the cell at the trailing edge:	$5.1 \cdot 10^{-3}c \times 5.2 \cdot 10^{-5}c$
Maximum aspect ratio:	440
Maximum i-stretching:	6.8%
Maximum j-stretching:	15%
Size of the computational domain:	$20c \times 20c \times 0.05c$

Table 1 Data on the 3.2 million nodes mesh.

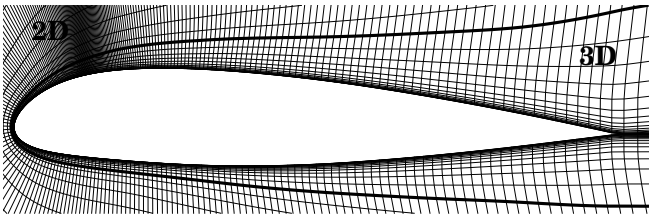

Fig. 3 The mesh with a focus of the resolution in the laminar and transitional region (1393×127 grid nodes). Every 4th node in each direction is shown.

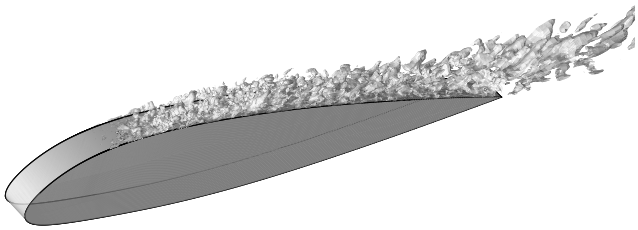

Fig. 4 Instantaneous w-velocity (contour levels at $w = 0.04U_\infty$).

streamwise grid spacing, Δx, is refined in the transition region as seen in Fig. 3. Also, the mesh is specially designed for this particular incidence with a refinement along the wake. The outer boundaries are located approximately ten chords away from the airfoil. The extent in the spanwise direction is chosen as $L_z = 0.05c$.

Boundary Conditions

The inflow condition is specified all over the curved area of the C-mesh. The velocities are set to $\overline{u} = U_\infty \cos\alpha$ and $\overline{v} = U_\infty \sin\alpha$, where U_∞ is the freestream velocity. At the outflow boundary, a convective boundary condition is applied: $\frac{\partial \overline{u}_i}{\partial t} + U_\infty \frac{\partial \overline{u}_i}{\partial x} = 0$. A Neumann boundary condition is used for the pressure at all boundaries ($\frac{\partial \overline{p}}{\partial n} = 0$) and periodic boundary conditions are used in the spanwise direction. The no-slip condition is used for the velocities at the wall. The freestream boundary value of k_{sgs}, k^∞_{sgs}, is set to a low value of $2.5 \cdot 10^{-8} U^2_\infty$. This gives a turbulence intensity, T', of 0.016%, where $T' = \sqrt{k^\infty_{sgs}/U^2_\infty}$. Dirichlet boundary conditions are used at the interfaces between the blocks. In the interface between the 2D and 3D domain the spanwise mean values are sent as Dirichlet conditions to the 2D domain.

Results

Computations

Two computations are presented in this paper. The computations have been performed on an IBM SP computer at the Center for Parallel Computing at KTH. The computational domain is decomposed into 36 subdomains. $4 \times 2 \times 4$ in the 3D domain and $4 \times 1 \times 1$ in the 2D domain. The elapsed time per time step on 36 processors is $30s$. The number of global iterations per time step is set to three. The L^1-norm of the residuals of the discretized momentum equations scaled with $\rho U_\infty A_{inlet} U_\infty$ is less than $8 \cdot 10^{-5}$ (A_{inlet} is the projected area of the inflow boundary). Here, the residuals are computed immediately after the solver (but without underrelaxation), i.e. the residuals are calculated with the 'old' coefficients and before the correction in the PISO algorithm. The L^1-norm of the discretized finite-volume continuity error scaled with the inlet mass flow is less than $3 \cdot 10^{-5}$. The simulation of one time unit (c/U_∞) requires about 3000 CPU hours and with MPI and 36 processors the solution is advanced 0.3 time units per day (24 hours). The averaging time is 2.9 time units for computation # 1 and 2.7 time units for computation # 2. The initial conditions are previous simulations, which originally were started from a 2D LES. The time step is $1 \cdot 10^{-4} c/U_\infty$, giving a maximum CFL number of 0.8.

The only set-up difference between the two computations is the treatment of the production term around the leading edge (see Table 2). The one-equation model is not able to model the transition (regarding the SGS stresses). A simulation was conducted where the production of k_{sgs} was suppressed around the leading edge. Within a radius of $0.15c$ the production term was linearly dampened to zero, i.e. $P_{k_{sgs}}$ in Eq. 5 is multiplied by $\min(1, r/0.15c)$, where r is the distance to origo, located at the very leading edge.

Computation	Modification of the production term
Computation # 1	No modification, i.e. $P_{k_{sgs}} = 2\nu_{sgs}\bar{S}_{ij}\bar{S}_{ij}$
Computation # 2	Blending within a radius of $0.15c$ around the l.e., i.e. $P_{k_{sgs}} = 2\nu_{sgs}\bar{S}_{ij}\bar{S}_{ij}\min(1, r/0.15c)$

Table 2 Treatment of the production term around the leading edge (l.e.).

Transition

The transition and growth of the turbulent boundary layer is clearly visualized in the computations, e.g. when looking at instantaneous contour plots of the resolved statistics. Fig. 4 shows the resolved velocity fluctuations in the spanwise direction.

The transition takes place in the reattachment region of the laminar separation bubble (see Fig. 5). Regarding the transition in total, also taking into account the SGS stresses, we can look at the total turbulent kinetic energy, k_t, defined as $k_t = k_{sgs} + \frac{u'^2+v'^2+w'^2}{2}$. The modification by Durbin effectively removes the SGS stresses in the stagnation point (not shown here). However, as we go around the leading edge, on the suction side, there are SGS stresses in the laminar region (the region with no resolved stresses), see Fig. 6. In the instantaneous plots (Figs. 5 and 6) it is clearly seen when the velocity starts to fluctuate. Figure 6 also shows the result of the modification of the production term in computation # 2: k_{sgs} is dampened close to origo, but still has a larger value between 9 and 12.5 % of the chord, compared with computation # 1. The question is what magnitude these stresses have compared with the resolved fluctuations further downstream. This is seen in Fig. 7: the lower lines are k_{sgs} and the lines collapse with k_t in the "laminar region" since the resolved velocity fluctuations are close to zero here. The magnitude of k_{sgs} in the "laminar region" is considerable, especially compared with k_{sgs} further downstream.

Figure 8 shows the pressure and skin friction coefficient. The pressure peak at the leading edge is slightly too low, but the pressure plateau, the decrease in the adverse pressure gradient, is reasonably well predicted at the trailing edge. Also the shape of the C_f looks reasonably good, downstream of the transition. Looking at the skin friction coefficient, the computations predict a laminar separation bubble, and then the skin friction increases, and the transition takes place. The predicted laminar separation bubble is too large giving the discrepancy in the pressure coefficient in the transitional region. The bubble is smaller in computation # 2. However, at the same time, the transition is slightly delayed compared with computation # 1. The overpredicted laminar separation bubbles result in a delayed transition. Comparing with Mary and Sagaut's results,[13] where they seem to have predicted the laminar and transitional regions in a physically correct way, they found the peak in c_f at $x = 0.16c$ ($c_f \approx 0.018$) and the maximum backflow skin friction was found to be approximately -0.006. In the present computations the bubble is too large with maximum backflow skin friction of approximately -0.013 and maximum peak at approximately 23 % of the chord ($c_f \approx 0.013$).

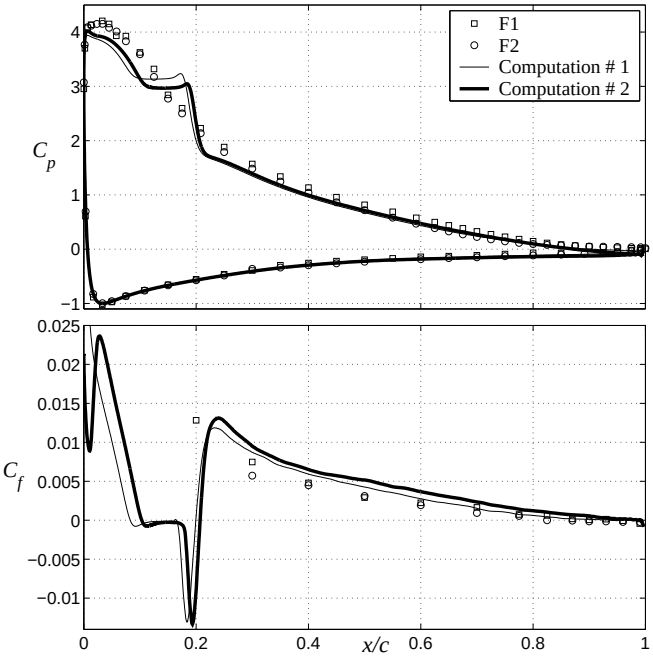

Fig. 8 Pressure and skin friction coefficients.

Looking at the skin friction coefficient for computation # 2 in Fig. 8, in the region near leading edge, where the SGS eddy viscosity is close to zero (see Figs. 6 and 7), the curve indicates that the laminar bubble would occur too soon, if the eddy viscosity would have been dampened even more. Instead, now, as the eddy viscosity starts to act (at $x \approx 0.025c$), the skin friction coefficient increases, peaks and starts to decrease, downstream compared to computation # 1. The contradictory results are: with the *present damping* the bubble is *delayed* and if zero eddy viscosity would have been used in the laminar region (that is *even more damping* would have been used), the bubble would probably occur *too early*. There is some inaccuracy in this region and perhaps it is important to have the correct freestream SGS turbulence levels to get the bubble at the correct location.

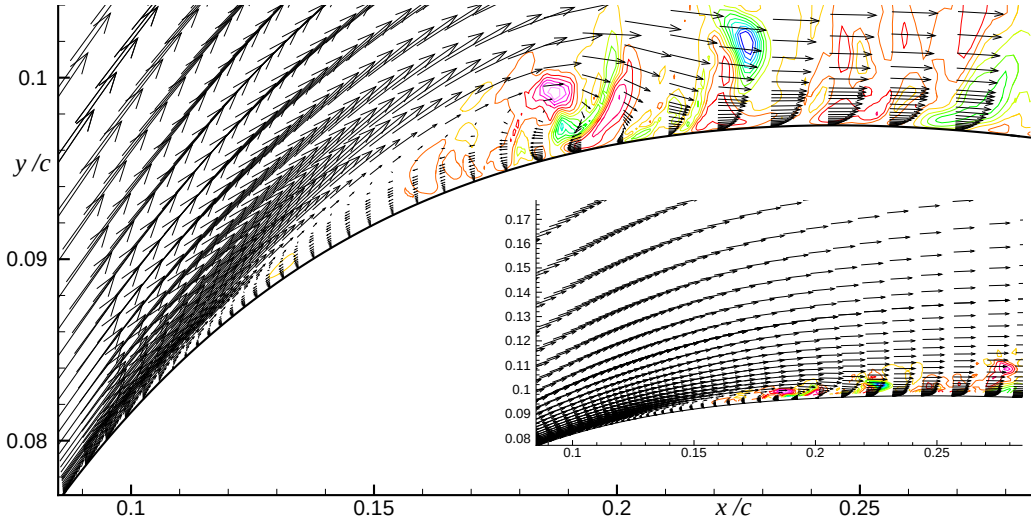

Fig. 5 Time and spanwise averaged velocity vectors and instantaneous $\overline{w}$-velocity contour plot. Every 10th node is shown in the streamwise direction and every 2nd in the wall-normal direction.

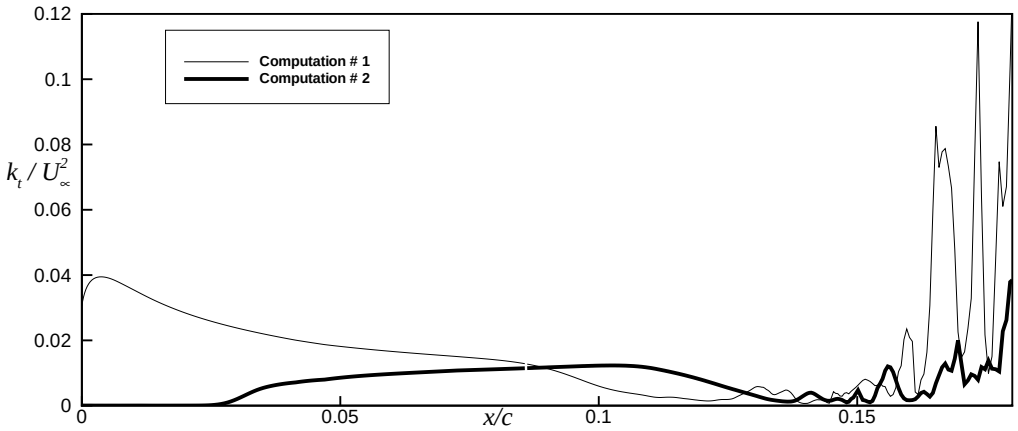

Fig. 6 Instantaneous total turbulent kinetic energy in the laminar/transitional region, roughly in the middle of the boundary layer ($j = 33$).

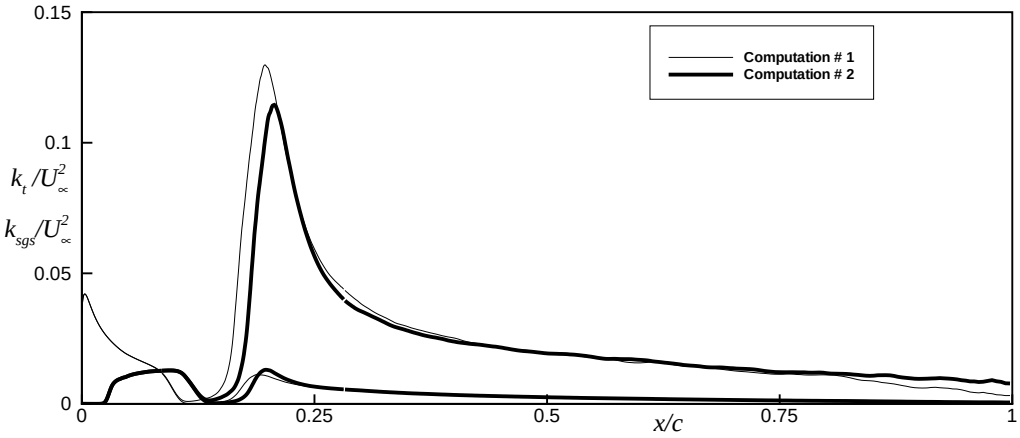

Fig. 7 Time and spanwise averaged total turbulent kinetic energy, k_t, roughly in the middle of the boundary layer ($j = 33$). Also shown are the mean kinetic energy of the unresolved stresses, k_{sgs} ($\leq k_t$).

	Exp. F1	Exp. F2	Comp. # 1	Comp. # 2
C_L	1.574	1.515	1.4672	1.5064
C_D	0.0212	0.0308	0.0329	0.0346

Table 3 Spanwise and time-averaged lift and drag coefficients for the computations and the experiments.

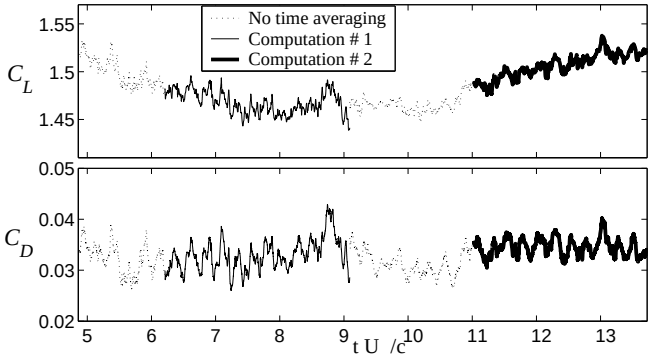

Fig. 9 Time history of the lift and drag coefficients.

Table 3 shows the lift and drag coefficients for the computations. The lift coefficients are underpredicted because of the failure to predict the laminar and transitional regions. Figure 9 show the time histories of the lift and drag coefficients for the computations. At $t = 0$ the LES was started from a 2D simulation. The regions where the time averaged results have been collected are shown in the figure. At $t \approx 9.1c/U_\infty$ the modification on the production term was added (computation # 2, see Table 2). The time averaging could be applied on longer signals, however since we have already concluded the problems with the transition, more exact values of the mean lift and drag coefficients are of little interest.

Figure 10 shows resolved velocity and stress profiles on the suction side of the airfoil and in the wake. The profiles of the streamwise velocity show that the boundary layer is too thick compared with the experiments. Comparing the two computations with one another, the delayed transition for computation # 2 seems to shift the streamwise velocity profiles all along the suction side. Looking at the stresses, they are too high in the beginning, much because of the delayed transition (it is in the transition region the fluctuations are at its peak). Further downstream the levels are too low, which is seen also in the wake.

The thickness of the boundary layer is connected to the size of the laminar separation bubble. Both the displacement and momentum thicknesses are smaller for computation # 2 (see Fig. 11). The displacement thickness is too thick downstream of the transition and happens to be in good agreement with the experiments for computation # 1 near the trailing edge. The momentum thickness

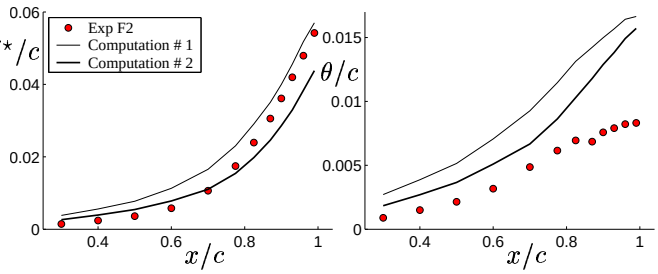

Fig. 11 Displacement and momentum thicknesses.

is too large, this is also seen in the velocity profiles as the shape of the profiles do not agree with the experiments. What we need to keep in mind though, is that the separation is milder in the experimental results from the F1 wind tunnel and our simulations agree more with those experiments. Unfortunately, no velocity profiles were measured in the F1 wind-tunnel case. A too large blockage of the experimental setup in the F2 wind tunnel is regarded as the main reason for the difference between the two experiments.[4] The different wind-tunnel measurements are compared with the simulations in Fig. 12. Here, in the bottom figure to the right, the pressure coefficients have been set to zero at $x = 0.9c$, to easy compare the shape of the curves, i.e. the level of the adverse pressure gradients in this region, close to the trailing edge.

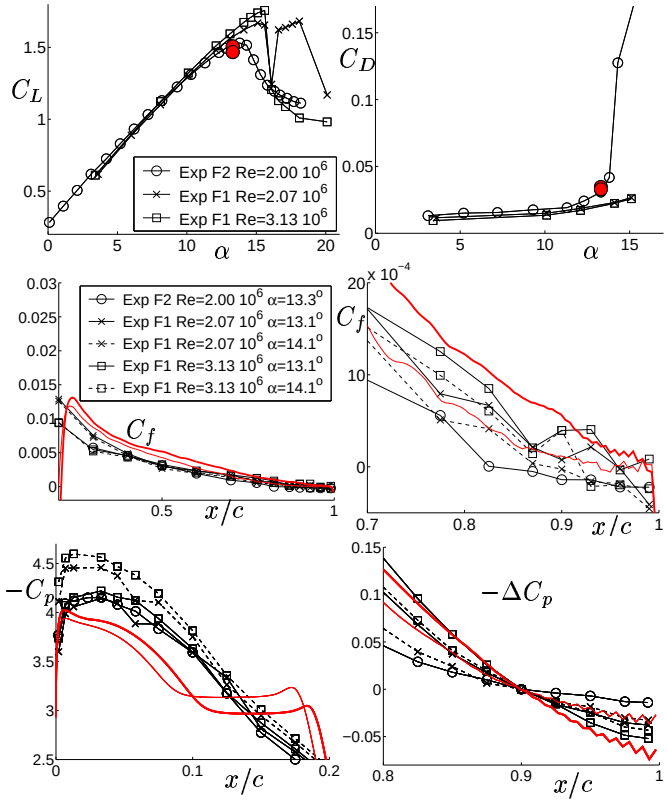

Fig. 12 Different experiments compared with the computations (the red lines and red markers).

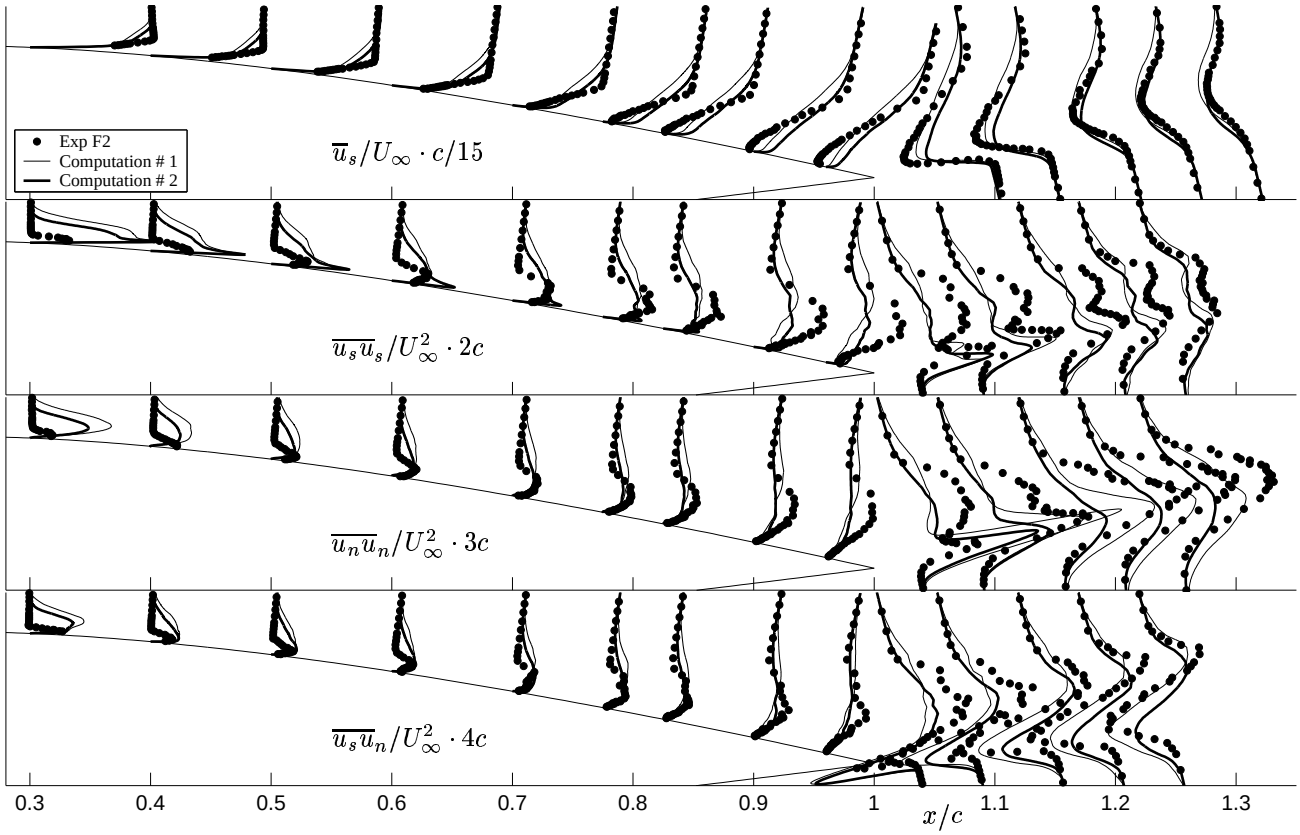

Fig. 10 Spanwise and time averaged first and second order statistics. Subscripts s and n denote the directions parallel and normal to the airfoil wall, respectively. The profiles are located at $x/c = 0.3$, 0.4, 0.5, 0.6, 0.7, 0.775, 0.825, 0.9 and 0.96. In the wake the subscripts s and n denote the directions parallel and normal to the freestream velocity, respectively. These profiles are located at $x'/c = 1.005$, 1.054, 1.119, 1.168 and 1.216, where $x' = \cos(\alpha)\, x$.

Resolution

The aim with the present mesh was to keep the resolution below 200 wall units in the streamwise and spanwise direction (Δx^+ and $\Delta z^+ < 200$). In the present computations the resolution (based on the predicted friction velocity) is less than 250 wall units (see Fig. 13). The spanwise resolution is coarse in the transition region and this might be further one reason for the overpredicted separation in this region.

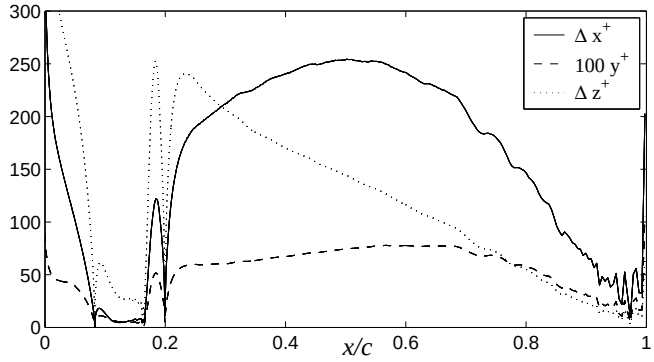

Fig. 13 Resolution along the suction side of the airfoil for computation # 1.

Figure 14 shows the mean blending factors in the spatial scheme (Eq. 9). In the wrap-around direction (streamwise or i- direction) the scheme is mostly central, except, as expected, in the stagnation point region. There is also a region on the pressure side near the trailing edge, where apparently there is a lot of wiggles. In the wall-normal direction, the scheme is mostly centered close to the wall. In the spanwise direction, the van Leer scheme is used in the laminar regions, where the magnitudes of the wiggles are very low and in future work this will be accounted for when constructing a new detector. Another improvement can be done at the block boundaries, where in the present computations van Leer always is used.

Figures 15-17 show two-point correlations, wavenumber and frequency spectra at three locations on the suction side of the profile. These spectral data are from computation # 2. The thick lines are data collected at the wall distance where the resolved energy is approximately maximal. The thin lines are data collected close to the wall. The resolution seems to be good. However looking at the frequency spectra at 90 % of the chord, the spectra have been collected for a too short period, in

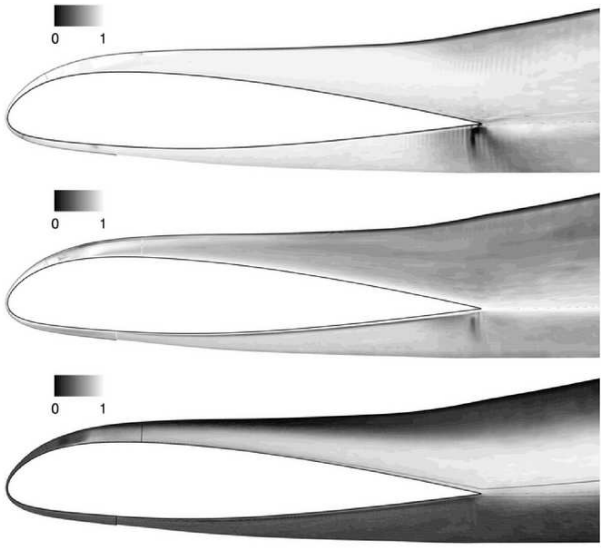

Fig. 14 From top to bottom: averaged blending factors in the streamwise, wall-normal and spanwise direction (i-, j- and k- direction) for computation # 2 in the 3D region.

order to get much information. Also, the maximum frequencies that are resolved are in the order of $U_{conv}/2\Delta x$. Here U_{conv} is the convective velocity at the point where the spectra are collected and e.g. at $x = 0.90c$ (Fig. 17) the highest frequencies resolved are approximately 35 at $y_n = 0.023c$ and 14 at $y_n = 0.0032c$. At 90 % of the chord (Fig. 17), the spanwise extent might not be quite sufficient. The velocities are correlated at the distance $z = 0.025c$ (especially for R_{vv} and R_{ww}). At 20 % of the chord (Fig. 15) the correlation length for $\overline{u}$, close to the wall (inside the separation bubble, at $y_n = 0.00058c$), is larger than $L_z/2$. A possible explanation might be the two-dimensional oscillations of the separation bubble.

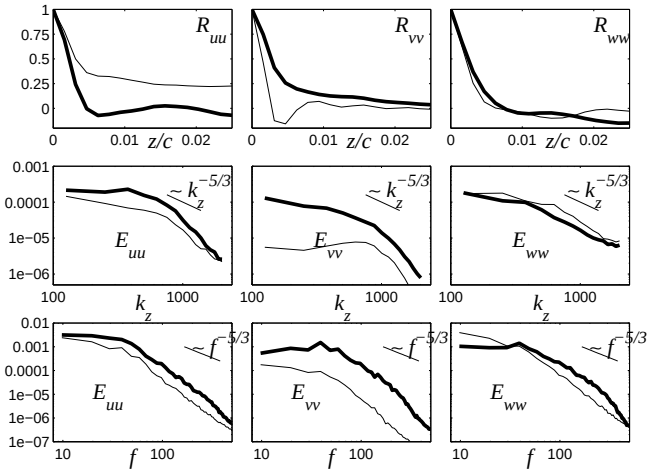

Fig. 15 Spanwise two-point correlations, wavenumber spectra and frequency spectra at $x/c = 0.20$ for computation # 2. Thick lines: at a wall distance of $y_n = 0.0048c$; thin lines: $y_n = 0.00058c$

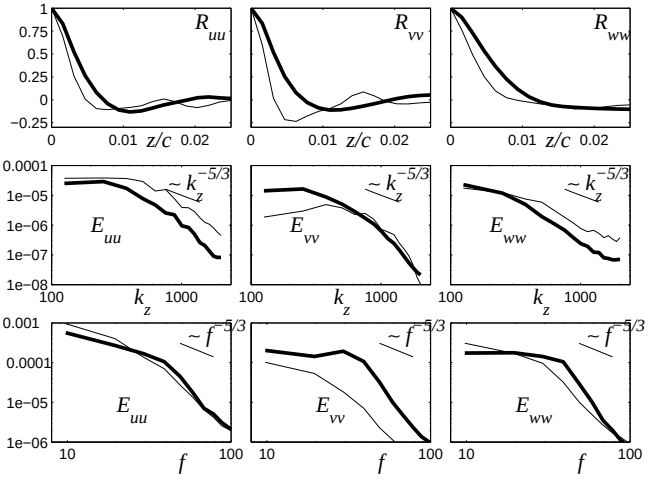

Fig. 16 Spanwise two-point correlations, wavenumber spectra and frequency spectra at $x/c = 0.60$ for computation # 2. Thick lines: at a wall distance of $y_n = 0.012c$; thin lines: $y_n = 0.0016c$

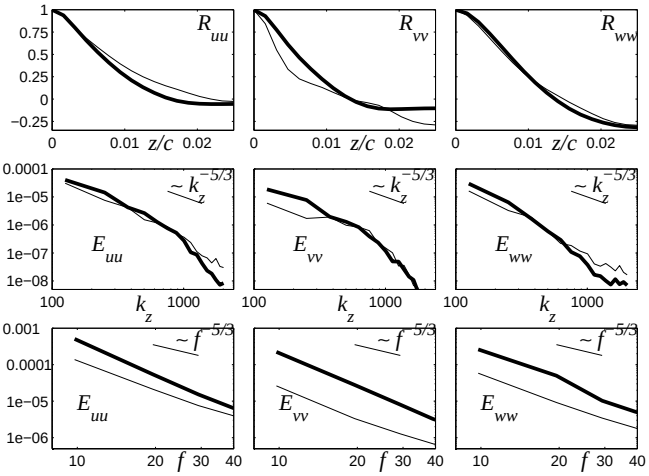

Fig. 17 Spanwise two-point correlations, wavenumber spectra and frequency spectra at $x/c = 0.90$ for computation # 2. Thick lines: at a wall distance of $y_n = 0.023c$; thin lines: $y_n = 0.0032c$

Conclusions and Future Work

The two computations presented in this paper differ only in the treatment of the laminar region, which has a major influence on the turbulent boundary layer further downstream. The importance of the transition must be stressed and there is more to do regarding the treatment of the laminar region. Encouraging is that the mechanism of the transition process seems to have been captured and that we get relatively good C_p and C_f profiles downstream of the transition. The modification by Durbin[26] removes the SGS stresses in the stagnation point region. However, there are SGS stresses in the laminar region on the suction side and the laminar separation bubble is too large resulting in an underpredicted lift coefficient. The SGS viscosity must be kept low in the laminar re-

gion. However the results also indicate that if zero eddy viscosity would have been used in the laminar region, the bubble would probably occur too early. This raises the question about the levels of the freestream SGS turbulence. To have the correct levels of the freestream SGS turbulence might be important and is what is missing in order to get the laminar bubble at the correct location.

The wiggle detector works fine and the unphysical oscillations are effectively dampened. Importantly, this scheme is mostly central in the turbulent boundary layer, perhaps owing to the resolution, which is less than 250 wall units. Also, the 2D/3D approach works fine and reduces the computational domain by 45 %, which leads to a great reduction in the computational time.

Spectra show that the resolution in the off-wall region is sufficient. Having a resolution less than 200 wall units seems like a good requirement. That is, we do have an LES in the off-near-wall region and since the transition mechanism seems to have been captured, perhaps the overall flow is reasonable and useful information could be obtained on e.g. the time variation of the lift and drag.

Overall, these are important conclusions and encouraging results, in order to continue investigating the coarse LES method. Although the transition is important, a near-wall model should also be added. The authors are presently working on such a model based on a one-equation RANS model[28] and the imposing of turbulent structures on the outer LES region. So far good results are obtained on channel flow and this model will also be tested on the airfoil using the coarse LES approach presented in this paper.

Acknowledgments

The LESFOIL project (Project No. BRPR-CT97-0565) was financed by the Brite-Euram programme. The interesting and stimulating discussions that always arose on the LESFOIL meetings are gratefully acknowledged. Finally, computer time at the IBM SP machine at PDC, Stockholm is acknowledged.

References

[1]Davidson, L., "LESFOIL: an European Project on Large Eddy Simulations around a High-Lift Airfoil at High Reynolds Number," *ECCOMAS 2000, European Congress on Computational Methods in Applied Sciences and Engineering, 11-14 September*, Barcelona, Spain, 2000.

[2]Davidson, L., Cokljat, D., Fröhlich, J., Leschziner, M., Mellen, C., and Rodi, W., editors, *LESFOIL- Large Eddy Simulation of Flow Around a High-Lift Airfoil*, Springer, 2002, In preparation.

[3]Mellen, C., Fröhlich, J., and Rodi, W., "Lessons from the European LESFOIL project on LES of flow around an airfoil," 40th Aerospace Sciences Meeting, AIAA Paper 2002-0111, Reno, 2002.

[4]Chaput, E., "Aerospatiale-A Airfoil. Contribution in ECARP- European Computational Aerodynamics Research Project: Validation of CFD Codes and Assessment of Turbulence Models," *Notes on Numerical Fluid Mechanics*, edited by W. H. *et* al., Vol. 58, Vieweg Verlag, 1997, pp. 327–346.

[5]Haase, W., Brandsma, F., Elsholz, E., Leschziner, M., and Schwamborn, D., editors, *EUROVAL- A European Initiative on Validation of CFD-codes*, Vol. 42, Vieweg Verlag, 1993.

[6]Haase, W., Chaput, E., Elsholz, E., Leschziner, M., and Müller, U., editors, *ECARP- European Computational Aerodynamics Research Project: Validation of CFD Codes and Assessment of Turbulence Models*, Vol. 58, Vieweg Verlag, 1997.

[7]Davidson, L. and Rizzi, A., "Navier-Stokes Stall Predictions Using an Algebraic Stress Model," *J. Spacecraft and Rockets*, Vol. 29, 1992, pp. 794–800.

[8]Davidson, L., "Prediction of the Flow Around an Airfoil Using a Reynolds Stress Transport Model," *ASME: Journal of Fluids Engineering*, Vol. 117, 1995, pp. 50–57.

[9]Lien, F. and Leschziner, M., "Modelling of 2D Separation from High-Lift Aerofoils With a Non-Linear Eddy-Viscosity Model and Second-Moment Closure," *The Aeronautical Journal*, Vol. 99, 1995, pp. 125–144.

[10]Kaltenbach, H.-J. and Choi, H., "Large-Eddy Simulation of Flow Around an Airfoil on a Structured Mesh," *Annual Research Briefs 1995*, Center for Turbulent Research, Stanford Univ./NASA Ames Reseach Center, 1995, pp. 51–60.

[11]Weber, C. and Ducros, F., "Large-eddy and Reynolds Averaged Navier-Stokes Simulations of turbulent flow over an airfoil," *Int. J. Comput. Fluid Dyn.*, Vol. 13, 2000, pp. 327–355.

[12]Held, J., *Large Eddy Simulation of Separated Compressible Flows around Wing Sections*, Ph.D. thesis, Dept. of Heat and Power Engineering, Lund Institute of Technology, Lund, 1999.

[13]Mary, I. and Sagaut, P., "Large Eddy Simulation of flow around an airfoil near stall," *AIAA Journal*, Vol. 40, No. 6, 2002, pp. 1139–1145.

[14]Mellen, C., Fröhlich, J., and Rodi, W., "Contribution by IfH in LESFOIL- Large Eddy Simulation of Flow Around a High-Lift Airfoil," *LESFOIL*, edited by L. Davidson, D. Cokljat, J. Fröhlich, M. Leschziner, C. Mellen, and W. Rodi, Springer, 2002, In preparation.

[15]Dahlström, S. and Davidson, L., "Large Eddy Simulation of the Flow around an Airfoil," 39th Aerospace Sciences Meeting, AIAA Paper 2001-0425, Reno, 2001.

[16]Voke, P., "Transition in LESFOIL- Large Eddy Simulation of Flow Around a High-Lift Airfoil," *LESFOIL*, edited by L. Davidson, D. Cokljat, J. Fröhlich, M. Leschziner, C. Mellen, and W. Rodi, Springer, 2002, In preparation.

[17]Cokljat, D. and Liu, F., "DES of turbulent flow over an airfoil at high incidence," 40th Aerospace Sciences Meeting, AIAA Paper 2002-0590, Reno, 2002.

[18]Dahlström, S. and Davidson, L., "Contribution by Chalmers in LESFOIL- Large Eddy Simulation of Flow Around a High-Lift Airfoil," *LESFOIL*, edited by L. Davidson, D. Cokljat, J. Fröhlich, M. Leschziner, C. Mellen, and W. Rodi, Springer, 2002, In preparation.

[19]Ducros, F., "Contribution by CERFACS in LESFOIL- Large Eddy Simulation of Flow Around a High-Lift Airfoil," *LESFOIL*, edited by L. Davidson, D. Cokljat, J. Fröhlich, M. Leschziner, C. Mellen, and W. Rodi, Springer, 2002, In preparation.

[20]Davidson, L. and Farhanieh, B., "CALC-BFC: A Finite-Volume Code Employing Collocated Variable Arrangement and Cartesian Velocity Components for Computation of Fluid Flow and Heat Transfer in Complex Three-Dimensional Geometries," Rept. 95/11, Dept. of Thermo and Fluid Dynamics, Chalmers University of Technology, Gothenburg, 1995.

[21]Rhie, C. and Chow, W., "Numerical Study of the Turbulent Flow Past an Airfoil With Trailing Edge Separation," *AIAA Journal*, Vol. 21, 1983, pp. 1525–1532.

[22]Nilsson, H. and Davidson, L., "CALC-PVM: A Parallel Multiblock SIMPLE Multiblock Solver for Turbulent Flow in

Complex Domains," Tech. Rep. 98/12, Dept. of Thermo and Fluid Dynamics, Chalmers University of Technology, Gothenburg, 1998.

[23]Issa, R., "Solution of Implicitly Discretised Fluid Flow Equations by Operator-Splitting," *J. Comp. Physics*, Vol. 62, 1986, pp. 40–65.

[24]Yoshizawa, A., "Statistical Theory for Compressible Shear Flows with the Application of Subgrid Modelling," *Physics of Fluids A*, Vol. 29, 1986, pp. 2152–2163.

[25]Fureby, C., "Large Eddy Simulation of Rearward-Facing Step Flow," *AIAA Journal*, Vol. 37, No. 11, 1999, pp. 1401–1410.

[26]Durbin, P. A., "On the $k-3$ stagnation point anomaly," *Int. J. Heat and Fluid Flow*, Vol. 17, 1996, pp. 89–90.

[27]Ferziger, J. and Peric, M., *Computational Methods for Fluid Dynamics*, Springer-Verlag, Berlin, 1996.

[28]Davidson, L., "Hybrid LES-RANS: A Combination of a One-equation SGS Model and a $k-\omega$ Model for predicting Recirculating Flows," *ECCOMAS CFD Conference*, Swansea, U.K., 2001.